*Progress In Electromagnetics Research C, Vol. 43, 15–28, 2013*

# SIMULATION AND ANALYSIS OF 60 GHz MILLIMETER-WAVE INDOOR PROPAGATION CHARACTERISTICS BASE ON THE METHOD OF SBR/IMAGE

**Yuan-Jian Liu, Qin-Jian Shi*, and Ye-Rong Zhang**

College of Electronic Science and Engineering, Nanjing University of Posts & Telecommunications, Nanjing, Jiangsu 210003, China

**Abstract**—In this paper, 60 GHz millimeter-wave indoor propagation characteristics are simulated and analyzed using the method of SBR/IM (shooting and bounding ray tracing/image). And the simulated and measured results agree well, so the correctness of the method has been validated. Some propagation parameters are obtained in the simulation, such as the indoor reception power distribution, distribution of phase angle of received power, root mean square (RMS) delay spread, direction of arrival, RMS angular spread, Doppler shift, etc. The analysis of the above results provides the foundation for the indoor coverage of millimeter-wave communication system.

## 1. INTRODUCTION

With the continuous development of wireless communications technology, spectrum occupancy is increasing. So it is necessary to develop microwave high-end spectrum resources to achieve high-speed broadband wireless communications. The most prominent advantage of millimeter wave is frequency bandwidth, and one percent of relative bandwidth of millimeter wave can provide available bandwidth to hundreds of megabytes or even gigabytes. It is particularly important to study the millimeter-wave propagation characteristics in the indoor environment, because millimeter-wave band communication is mainly used in office, laboratory, etc [1–3]. The models of study on the indoor propagation characteristics can be divided into two categories: empirical and deterministic models [4]. The empirical model is based on simple formulas, so it only requires simple inputs, and its operation is very fast. However, the model requires precise equipment, and some

*Received 1 June 2013, Accepted 31 July 2013, Scheduled 23 August 2013*

* Corresponding author: Qin-Jian Shi (ud3776034@126.com).

useful propagation parameters cannot be obtained in the measure, such as direction of arrival, distribution of the direction angle of arrival and angular spread. Thus this model has significant limitation on the study of radio channel [5]. The deterministic model is based on the theory of electromagnetic wave propagation, and two methods are generally used: ray tracing method and finite difference time domain method. In recent years, ray tracing method has been used to predict the indoor propagation characteristics because of the improvement of the calculation ability of computer.

Ray tracing method includes image method, minimum optical path method, test-ray method, shooting and bounding ray tracing method, deterministic ray tube method and shooting and bounding ray tracing/image method (SBR/IM). The image method [6, 7] is a simple ray tracing method because it does not need to do the intersection test. But it can only be applied to a simple structure of the environment. The minimum optical path method [8] is essentially the same as the traditional image method. This method does not use reflection law but the minimum optical path to determine the location of the reflection point of wall. It cannot be applied to complex environment either. The test ray method [9] does not need to determine the location of the point of the receiver in advance, but it needs receiving ball. It can be applied to the complex environment, but the prediction accuracy of this method is affected by the radius of receiving ball. So the calculated efficiency is not high. The shooting and bounding ray tracing method [10] does not need receiving ball, but this method takes up a lot of computer resources. The deterministic ray tube method [11] saves computer resources, but it needs to create a ray tree based on the actual environment, and it is complex. The shooting and bounding ray tracing/image method [12, 13] can be used for any complex propagation environment, and it can find all the radio wave propagation paths from the transmitter to the receiver with high accuracy and computational efficiency. So this method is a valuable method which can be used to predict the radio wave propagation. In this paper, 60 GHz millimeter-wave indoor propagation characteristics are simulated based on the shooting and bounding ray tracing/image method.

## 2. THE REALIZATION OF SBR/IM

### 2.1. Indoor Structure Representation

Indoor building structure will be simplified, and the geometry data and form data of each plane will be recorded while every face is given a unique identifier to represent the plane. Then data are entered

into the database in accordance with the prescribed format, and the appropriate priority list will be established.

### 2.2. Wavefront Generation

The radio beams radiated by the transmit antenna can be deemed many ray tubes. The wavefront ball should be divided to generate the ray tubes, and the shape and size of each wavefront are the same. The shape of wavefront can be an equilateral triangle, quadrilateral or hexagonal. In this paper, a common method is used to divide the wavefront ball. A regular icosahedron in the interior of wavefront ball is shown in Fig. 1, and twelve vertex coordinates of the regular icosahedron can be calculated [14].

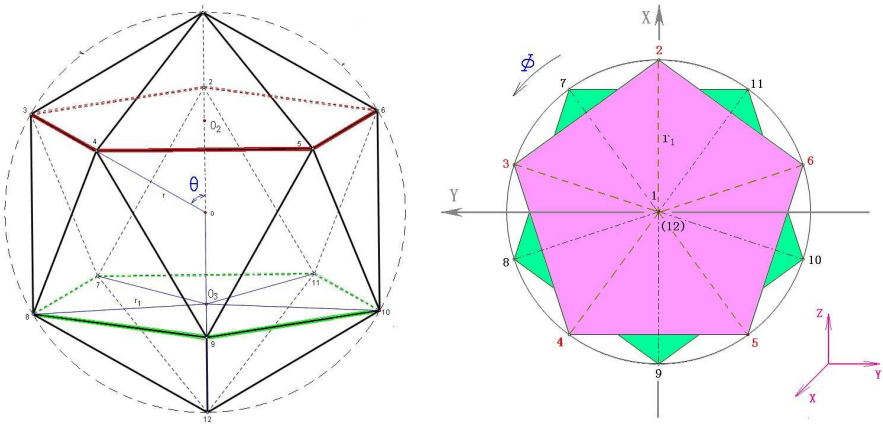


**Figure 1.** Regular icosahedron in the interior of wavefront ball.

### 2.3. The Establishment of the Emitted Ray Tubes

The tetrahedral ray tube with sections of equilateral triangles is shown in Fig. 2 [14, 15].

### 2.4. Intersection Test

The model of intersection test is shown in Fig. 3 [14, 15].

### 2.5. The Determination of Reflected Ray Tubes

The image source point can be located using the image method, and three intersection points of three rays of the emitted ray tube and plane

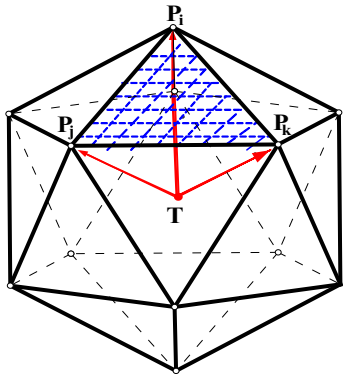


**Figure 2.** Establishment of the emitted ray tube.

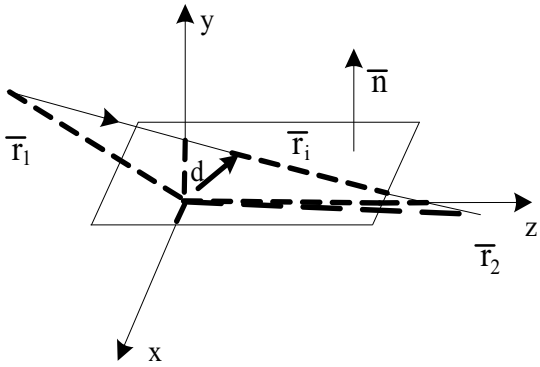


**Figure 3.** The model of intersection test.

can be determined. So the reflected ray tubes will be obtained by the four points.

### 2.6. The Determination of Ray Tubes Which Reach the Received Point

Figures 4 and 5 are the schematic diagrams of the determination of ray tubes which reach the received point [14, 15].

### 2.7. Calculation of Received Field

The received field is the vector sum of the ray tubes filed which can reach the receiving point [14, 15].

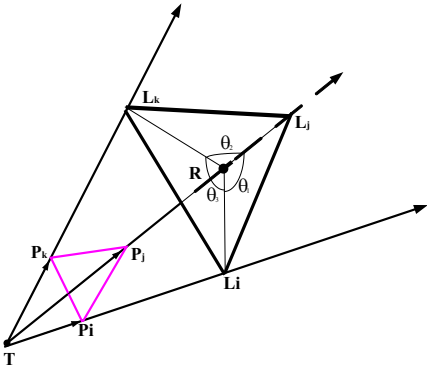


**Figure 4.** Schematic diagram of receiving point.

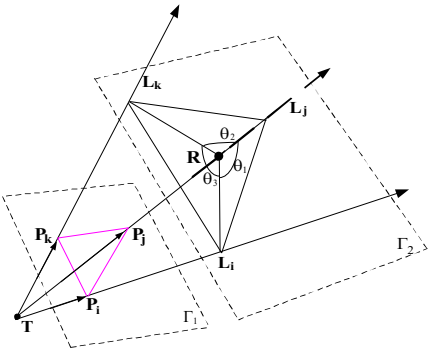


**Figure 5.** Schematic diagram of judgment method.

(1) The calculation formula of the direct field is $\overrightarrow{E} = \overrightarrow{E}_0 \cdot \frac{e^{-jk|TR|}}{|TR|}$. $\overrightarrow{E}_0$ is the electric filed value of ray tube $T - P_iP_jP_k$ in the reference position $\Delta P_iP_jP_k$, and $k$ is wave number. $|TR|$ is the actual propagation distance when the ray tube $T - P_iP_jP_k$ reaches received point $R$.

(2) The calculation formula of the reflected field is $\overrightarrow{E} = \overrightarrow{E}_0 \cdot \{\Pi\overline{\overline{R}_i}\} \cdot \{\Pi\overline{\overline{T}_i}\} \cdot \{\Pi e^{-\gamma_i l_i}\} \cdot SF$. $\{\Pi\overline{\overline{R}_i}\}$ is the dyad of the reflection coefficient, $\bar{\bar{R}}_i = R_{i\perp}\bar{e}_\perp\bar{e}_\perp + R_{i\parallel}\bar{e}_\parallel\bar{e}_\parallel$, $R_{i\perp} = \frac{\cos\theta_i - \sqrt{\varepsilon_2/\varepsilon_1 - \sin^2\theta_i}}{\cos\theta_i + \sqrt{\varepsilon_2/\varepsilon_1 - \sin^2\theta_i}}$, $R_{i\parallel} = \frac{(\varepsilon_2/\varepsilon_1)\cos\theta_i - \sqrt{\varepsilon_2/\varepsilon_1 - \sin^2\theta_i}}{(\varepsilon_2/\varepsilon_1)\cos\theta_i + \sqrt{\varepsilon_2/\varepsilon_1 - \sin^2\theta_i}}$. $\left\{\Pi\overline{\overline{T}_i}\right\}$ is the dyad of the transmission coefficient, $\overline{\overline{T_i}} = T_{i\perp}\bar{e}_\perp\bar{e}_\perp + T_{i\parallel}\bar{e}_\parallel\bar{e}_\parallel$, $T_{i\perp} = R_{i\perp} + 1$, $T_{i\parallel} = (R_{i\parallel} + 1) \cdot \sqrt{\varepsilon_1/\varepsilon_2}$. $\gamma_i$ is the phase change relative to the reference position $\Delta P_iP_jP_k$ and the $l_i$ is the attenuation change relative to the reference position. $SF$ is the diffusion factor, and the calculation formula is $SF = \frac{\sqrt{S_{\Delta L_iL_jL_k}}}{\sqrt{S_{\Delta P_iP_jP_k}}}$, $S_{\Delta L_iL_jL_k}$ is area of triangle $\Delta L_iL_jL_k$, $S_{\Delta p_ip_jp_k}$ is area of triangle $\Delta P_iP_jP_k$.

## 3. NUMERICAL RESULTS

The simulation environment in [16] is a room with dimensions $14.5 \times 9.9 \times 2.6$, as shown in Fig. 6. The ceiling is made of gypsum board, and the floor is made of resin. In the simulation, vertically polarized omnidirectional antennas with 5 dBi of gain are used, and the heights

of transmitter antenna and receiver antenna are 2.2 m and 1.2 m, respectively. The frequency of transmitted signal is 59.5 GHz, and the transmission power is 10 dBm. The transmitter antenna is in the center of the room, and the receiver antenna moves along a straight line. The electromagnetic properties of all materials are given in Table 1.

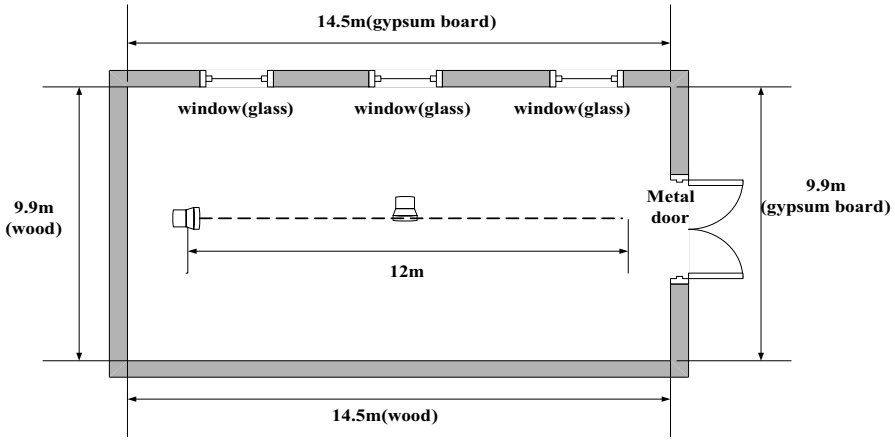


**Figure 6.** Simulation environment.

**Table 1.** Electromagnetic properties of different materials.

| Material | Electromagnetic property | |
|---|---|---|
| | $\varepsilon_r$ | $\sigma$ |
| Wood | 5.0 | 0.001 |
| Glass | 2.4 | 0.001 |
| Gypsum board | 2.8 | 0.150 |
| Resin | 4.0 | 0.001 |

### 3.1. Correctness Verification

Simulated and measured results in [16] agree well as shown in Fig. 7, so the correctness of the method has been validated. And Fig. 9 shows the difference between the simulated and measured results at both ends. The following is the reason for the difference. (1) There is a difference of electromagnetic property between the simulation and actual material. (2) It cannot be assured that the movement of receiver

is completely a straight line in the measure. (3) There is a difference in the size of simulation room between the simulation and actual room. (4) The number of received points in the measure is smaller than in the simulation.

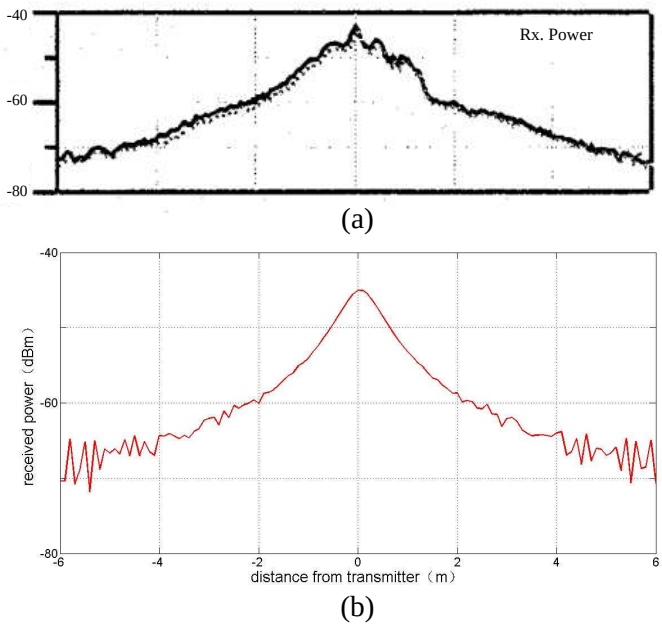


**Figure 7.** Received power: (a) Measured result in literature [16], (b) simulated result.

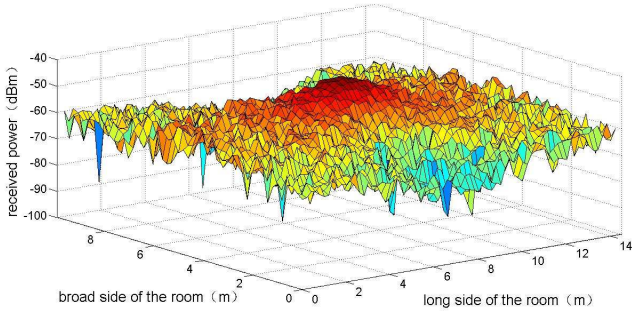


**Figure 8.** The distribution of received power.

### 3.2. The Distribution of Received Power

As shown in Fig. 8, the received power in the intermediate position is significantly higher than the other position, and the received power on the edge of the room is low because the transmitter antenna is in the center of the room. The received power of the direct path accounts for a large part of the total received power. But the distribution of received power is not completely inversely proportional to the distance from the transmitter antenna. It is shown that there are reflected paths and diffraction paths besides the direct path in the process of propagation. Fig. 9 shows the statistical distribution of phase angle of received power which is in uniform distribution.

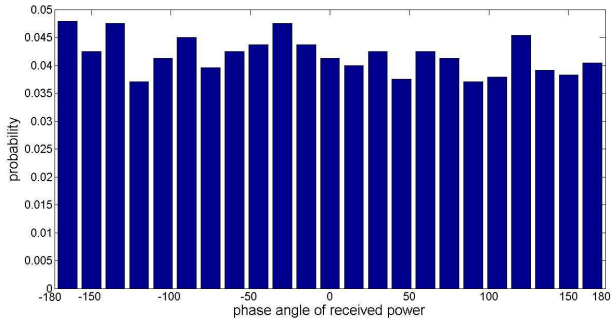


**Figure 9.** The phase angle of received power.

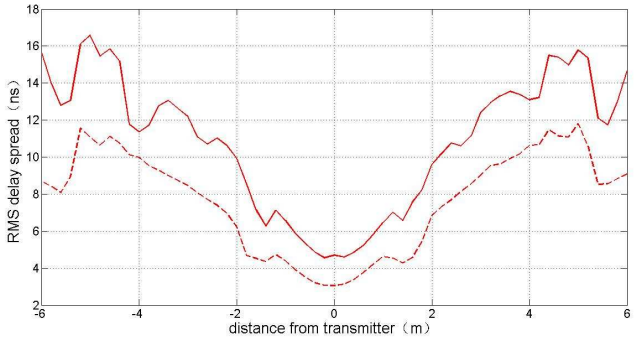


**Figure 10.** The RMS delay spread (The solid line is the result using omnidirectional antenna, and the dotted line is the result using directive antenna).

### 3.3. The Root Mean Square (RMS) Delay Spread

Figure 10 shows the RMS delay spread of millimeter-wave in an indoor environment. The solid line is the RMS delay spread using omnidirectional antenna, and the dotted line is the result using directive antenna. The RMS delay spread is the second moment of power delay profile, and it is defined as:

$$\sigma = \sqrt{\frac{\sum_{i=1}^{N_p} P_i t_i^2}{P_R} - \bar{t}^2}$$

$\bar{t}$ is the average time of arrival and defined as $\bar{t} = \frac{\sum_{i=1}^{N_p} P_i t_i}{P_R}$. $P_i$ is the received power of the $i$th path and $P_R$ the total of received power. The RMS delay spread is a better measure of the spread of multipath, and it varies in the level of ns [14].

In this paper, the RMS delay spread of millimeter-wave varies between 4.8 ns and 16.6 ns as shown in Fig. 10. The worst RMS delay spread occurs at the distance of $-5$ m and 5 m, which is close to the

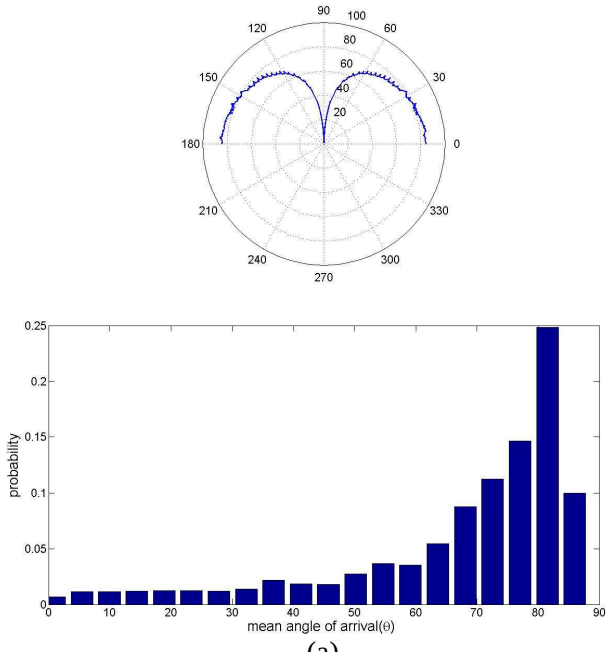


(a)

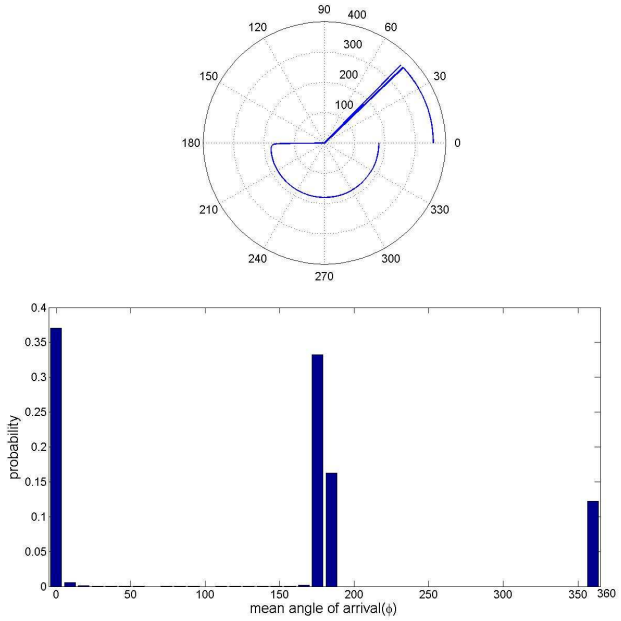


(b)

**Figure 11.** Mean angle of arrival: (a) Mean angle of arrival $\bar{\theta}$, (b) mean angle of arrival $\bar{\phi}$.

edge of the room, and the least RMS delay spread occurs at the distance of 0 m which is just below the transmitter antenna. This is because when the receiver antenna is just below the transmitter antenna, there are almost only reflected paths from surface of the floor and ceiling besides the direct path. And the RMS delay spread can be reduced about 2 ns–4 ns by using a directive antenna to suppress reflections from surface of floor and ceiling.

### 3.4. The Direction of Arrival and RMS Angular Spread

The direction of arrival which is defined as $\bar{a} = \sin(\theta_A)\cos(\phi_A)\bar{x} + \sin(\theta_A)\sin(\phi_A)\bar{y} + \cos(\phi_A)\bar{z}$ can be obtained.

Figure 11 shows the mean angle of arrival of all the received point. The $\bar{\theta}$ is defined as $\bar{\theta} = \tan^{-1}(\frac{\sqrt{A_x^2+A_y^2}}{A_z})$, and the $\bar{\phi}$ is defined as $\bar{\phi} = \cos^{-1}(\frac{A_y}{A_x})(A = \sum_{i=1}^{N} P_i\bar{a})$.

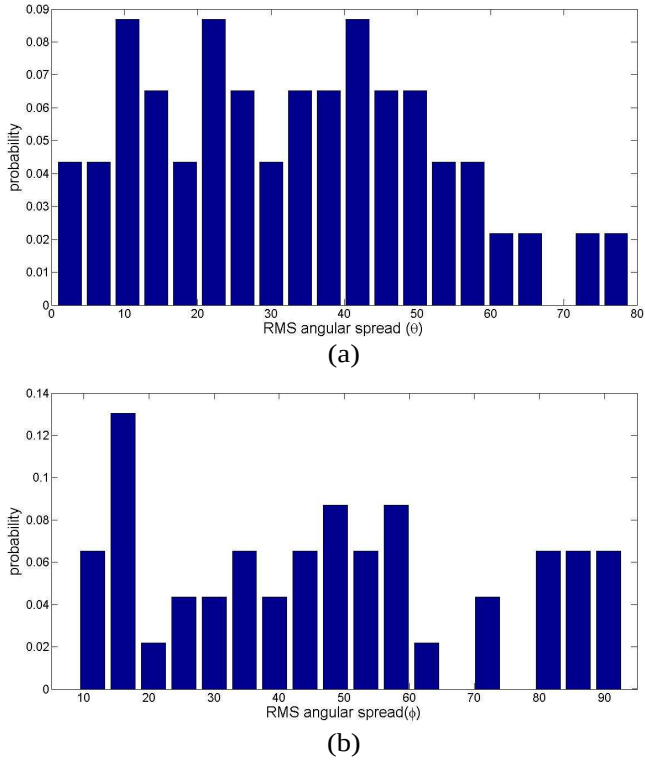


**Figure 12.** RMS angular spread: (a) RMS angular spread ($\bar{\theta}$), (b) RMS angular spread ($\bar{\phi}$).

Figure 12 shows the RMS angular spread. The RMS angular spread ($\bar{\theta}$) varies between 0°–80°. The RMS angular spread ($\bar{\phi}$) varies between 10°–90°.

### 3.5. Doppler Shift

The formula of Doppler shift is $\Delta f = f_0[\frac{\bar{d}\cdot\overline{V_T}+\bar{a}\cdot\overline{V_R}}{c}]$. So each path will cause the Doppler shift when the transmitter or the receiver is moving. So the Doppler shift can be determined (Assuming that the transmitter is fixed and that the speed of receiver is 1 m/s). The Doppler shift varies between −800 Hz and 800 Hz as shown in Fig. 13. This simulation environment is similar to indoor mobile communication environment, so the range of Doppler shift in this simulation provides the theoretical foundation for the indoor coverage of millimeter-wave communication system.

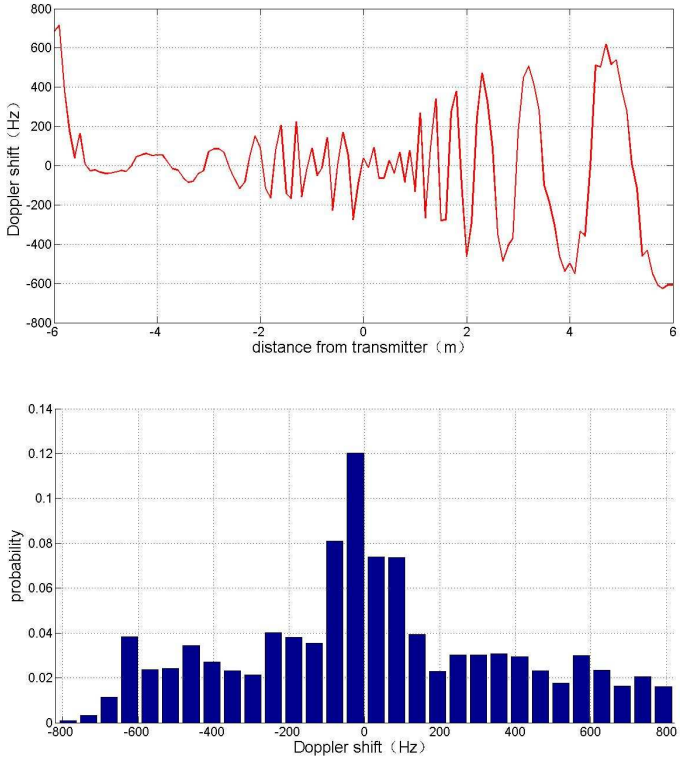


**Figure 13.** Doppler shift.

## 4. CONCLUSIONS

In this paper, the 60 GHz millimeter-wave indoor propagation characteristics are simulated and analyzed using the method of SBR/IM. And the simulated and measured results are in good agreement, so the correctness of the method has been validated. The received power of the direct path accounts for a large part of the total received power. The RMS delay spread of millimeter-wave varies between 4.8 ns and 16.6 ns in this simulation, and the RMS delay spread can be reduced about 2 ns–4 ns by using a directive antenna. Assuming that the transmitter is fixed and the speed of receiver is 1 m/s, the Doppler shift will vary between −800 Hz and 800 Hz. The analysis of the above results provides a foundation for the indoor coverage of millimeter-wave communication system. This simulation environment is almost an empty room. However, the actual indoor environment

is not as simple as the simulation environment. Millimeter wave propagation characteristics in complex indoor environments require further analysis, which is our next research direction.

## REFERENCES

1. Hammoudeh, A. K., "Millimetric wavelengths radiowave propagation for line of sight indoor microcellular mobile communications," *IEEE Transactions on Vehicular Technology*, Vol. 3, No. 44, 449–460, 1995.
2. Wang, Y.-Z., L.-J. Li, and K. Gong, "A study on millimeter-wave indoor propagation characteristics," *Chinese Journal of Electronics*, Vol. 27, No. 3, 89–93, 1999.
3. Smulders, P., "Exploiting the 60 GHz band for local wireless multimedia access: Prospects and future directions," *IEEE Communications Magazine*, Vol. 40, No. 1, 140–147, 2002.
4. Yang, D.-C., *Mobile Propagation Environment*, 121–122, China Machine Press, 2003.
5. Li, C.-F. and P.-N. Jiao, "Experimental verification of a ray tracing model at 5.8 GHz," *Chinese Journal of Radio Science*, Vol. 21, No. 6, 921–924, 2006.
6. Tan, S. Y. and H. S. Tan, "A microcellular communications propagation model based on the uniform theory of diffraction and multiple image theory," *IEEE Transactions on Antennas Propagation*, Vol. 44, No. 10, 1317–1326, 1996.
7. Grubisic, S., "Ray-tracing propagation model using image theory with a new accurate approximation for transmitted rays through walls," *IEEE Transactions on Antennas Propagation*, Vol. 42, No. 4, 835–838, 2006.
8. Sanchez, M. G., "Exhaustive ray tracing algorithm for microcellular propagation prediction models," *Electronics Letters*, Vol. 7, No. 32, 624–625, Mar. 1996.
9. Honcharenko, W., "Mechanisms governing UHF propagation on single floors in modern office buildings," *IEEE Transactions on Antennas Propagation*, Vol. 4, No. 41, 496–504, 1992.
10. Sato, H. S. and K. Otoi, "Electromagnetic wave propagation estimation by 3-D SBR method," *Electromagnetics in Advanced Applications, ICEAA*, 129–132, 2007.
11. Son, H. W. and N. H. Myung, "A deterministic ray tube method for microcellular wave propagation prediction model,"

*IEEE Transactions on Vehicular Technology*, Vol. 47, No. 8, 1344–1350, 1999.

12. Chen, S. H. and S. K. Jeng, "SBR image approach for radio wave propagation in tunnels with and without traffic," *IEEE Transactions on Antennas and Propagation*, Vol. 3, No. 45, 570–578, 1996.
13. Chen, S. H., "An SBR/image approach for radio wave propagation in indoor environments with metallic furniture," *IEEE Transactions on Antennas and Propagation*, Vol. 1, No. 45, 98–106, 1997.
14. Wu, Z.-Z., *The Wireless Radio Propagation of Mobile Communication*, 258–261, The Publishing Company of People Post and Telecommunications, 2002.
15. Liu, Y.-J., H. Chen, Y.-R. Zhang, and W. Cao, "Design of software predicting indoor microcell field strength," *Journal of Nanjing University of Posts and Telecommunications*, Vol. 27, No. 5, 1–5, 2007.
16. Kato, A., T. Manade, Y. Miura, K. Sato, and T. Ihara, "Measurements of millimeter wave indoor propagation and high-speed digital transmission characteristics at 60 GHz," *The 8th IEEE International Symposium*, Vol. 1, 149–154, 1997.